Time-resolved ring structure of circularly polarized beams backscattered from forward scattering media

Kevin G. Phillips, Min Xu, S.K. Gayen, R.R. Alfano

Institute for Ultrafast Spectroscopy and Lasers, Department of Physics, City College of New York, Graduate School of the City University of New York, New York, New York 10031

kevphill@sci.ccny.cuny.edu

Abstract: The backscattering of circularly polarized light at normal incidence to a half-space of scattering particles is studied using the Electric Field Monte Carlo (EMC) method. The spatial distribution of the backscattered light intensity is examined for both the time-resolved and continuous wave cases for large particles with anisotropy factor, g, in the range 0.8 to 0.97. For the time-resolved case, the backscattered light with the same helicity as that of the incident beam (co-polarized) is found to form a ring centered on the point of incidence. The ring expands and simultaneously grows weak as time increases. The intensity of backscattered light with helicity opposite to that of the incident beam (cross-polarized) is found to exhibit a ring behavior for $g \geq 0.85$, with significant backscattering at the point of incidence. For the continuous-wave case no such ring pattern is observed in backscattered light for either helicity. The present EMC study suggests that the ring behavior can only be observed in the time domain, in contrast to previous studies of light backscattered from forward scattering media based on the scalar time-independent Fokker-Planck approximation to the radiative transfer equation. The time-dependent ring structure of backscattered light may have potential use in subsurface imaging applications.

OCIS codes: (290.1350) Backscattering; (170.3660) Light propagation in tissues; (290.4210) Multiple scattering; (030.5620) Radiative transfer; (170.6920) Time-resolved imaging

References and links

1. G. D. Gilbert and J. C. Pernicka, "Improvement of underwater visibility by reduction of backscatter with a circular polarization technique," Appl. Opt. **6**, 741-746 (1967).
2. G. D. Lewis, D. L. Jordan and P. J. Roberts, "Backscattering target detection in a turbid medium by polarization discrimination," Appl. Opt. **38**, 3937-3944 (1999).
3. S. P. Morgan and M. E. Ridgway, "Polarization properties of light backscattered from a two layer scattering medium," Opt. Express **7**, 395-402 (2000).
4. X. Ni and R. R. Alfano, "Time-resolved backscattering of circularly and linearly polarized light in a turbid medium," Opt. Lett. **29**, 2773-2775 (2004).
5. M. Xu and R. R. Alfano, "Circular polarization memory of light," Phys. Rev. E (submitted for publication)
6. F. C. MacKintosh, J. X. Zhu, D. J. Pine and D. A. Weitz, "Polarization memory of multiply scattered light," Phys. Rev. B **40**, R9342-R9345 (1989).
7. A. D. Kim and M. Moscoso, "Backscattering of beams by forward-peaked scattering media," Opt. Lett. **29**, 74-76 (2004).

#8479 - $15.00 USD Received 18 August 2005; revised 19 September 2005; accepted 19 September 2005

8. Min Xu, "Electric field Monte Carlo simulation of polarized light propagation in turbid media," Opt. Express **12**, 6530-6539 (2004).
9. A. Ishimaru, *Wave propagation and scattering in random media, I and II* (Academic, New York, 1978).
10. S. Chandrasekhar, *Radiative transfer* (Oxford University Press, Oxford, UK, 1960).
11. K. F. Evans and G. L. Stephens, "A new polarized atmospheric radiative transfer model," J. Quant. Spectrosc. Radiat. Transfer **46**, 413-423 (1991).
12. A. D. Kim and M. Moscoso, "Chebyshev spectral methods for radiative transfer," SIAM J. Sci. Comput. **23**, 2074-2094 (2002).
13. G. W. Kattawar and G. N. Plass, "Radiance and polarization of multiply scattered light from haze clouds," Appl. Opt. **7**, 1519-1527 (1968).
14. I. Lux and L. Koblinger, *Monte Carlo particle transport methods: neutron and photon calculations* (CRC Press, Boca Raton, Fla., 1991).
15. J. M. Schmitt, A. H. Gandjbakhche and R. F. Bonner, "Use of polarized light to discriminate short-path photons in a multiply scattering medium," Appl. Opt. **31**, 6535-6546 (1992).
16. P. Bruscaglioni, G. Zaccanit and Q. Wei, "Transmission of a pulsed polarized light beam through thick turbid media: numerical results," Appl. Opt. **32**, 6142-6150 (1993).
17. M. J. Rakovic, G. W. Kattawar, M. Mehrbeolu, B. D. Cameron, L. V. Wang, S. Rastegar and G.L. Cote, "Light backscattering polarization patterns from turbid media: theory and experiment," Appl. Opt. **38**, 3399-3408 (1999).
18. S. Bartel and A. H. Hielscher,"Monte Carlo simulations of the diffuse backscattering Mueller matrix for highly scattering media," Appl. Opt. **39**, 1580-1588 (2000).
19. M. Moscoso, J. B. Keller and G. Papanicolaou, "Depolarization and blurring of optical images by biological tissue," J. Opt. Soc. Am. A **18**, 948-960 (2001).
20. H. H. Tynes, G. W. Kattawar, E. P. Zege, I. L. Katsev, A. S. Prikhach and L. I. Chaikovskaya, "Monte Carlo and multicomponent approximation methods for vector radiative transfer by use of effective Mueller matrix calculations ," Appl. Opt. **40**, 400-412 (2001).
21. R. Y. Rubinstein, *Simulation and the Monte Carlo method* (John Wiley and Sons, 1981)

1. Introduction

Polarized light backscattered from highly scattering media carries medium-specific information that can be utilized in polarization sensitive imaging techniques [1]-[4]. How light depolarizes and propagates from and within a scattering medium remains an active topic of research in optical imaging of targets embedded in highly scattering media. Polarization sensitive imaging techniques depend on the level of anisotropy of the scattering medium, which in turn depends on the relative size of scattering particle and wavelength of light used. When the particle diameter, a, is small compared to the wavelength, λ, of incident light, the transport mean free path, l_t, becomes equal to the scattering mean free path, l_s, and isotropic scattering results. In isotropic scattering linearly polarized light has a longer depolarization length than circularly polarized light and tends to backscatter with the same polarization as the input whereas circularly polarized light backscatters with its helicity flipped. This is attributed to single scattering events with large scattering angle. In the case of anisotropic scattering for large particles, where $a \geq \frac{\lambda}{4}$ yielding $l_t > l_s$, circularly polarized light has a longer depolarization length than linearly polarized light and backscatters with preserved helicity [5]. This process is termed polarization memory [6]. In this case linearly polarized light is backscattered with some elliptic polarization. This is attributed to forward scattering within the medium, causing the polarization of linearly polarized light to become randomized over shorter distances than the circularly polarized light.

The questions that need to be addressed include the following. Is light backscattered primarily from the point of incidence? Does backscattered light take special pathways inside the media towards the incident surface? Does the backscattered light exhibit time-dependent features? These questions warrant study as it is strongly anisotropic scattering in the forward direction that is encountered in biomedical optical imaging. Such knowledge would give an indication of the scattering behavior of light as it travels *inside* the scattering medium.

An analysis of the spatial dependence of backscattered circularly polarized beams was first carried out by Kim and Moscoso [7] who used the scalar time-independent Fokker-Planck

#8479 - $15.00 USD Received 18 August 2005; revised 19 September 2005; accepted 19 September 2005

equation, an approximation to the radiative transfer equation. They predict a time-independent circularly symmetric peak centered on the point of incidence, henceforth referred to as a "ring" or "ring-peak", in the backscattered light and postulate that light comprising the ring is of the same helicity as the circularly polarized incident beam.

In this study, the Electric Field Monte Carlo method [8] is used to investigate the spatial distribution of time-dependent (time-resolved), in addition to steady state (continuous wave), properties of light backscattered when a pencil-like beam is incident on a half-space of forward scattering particles whose anisotropy factors range from $g = 0.8$ to $g = 0.97$. The EMC program uses the exact phase function of the individual scatterers to allow for a more physical simulation of light propagation. The EMC simulation results suggest that the backscattered light forms rings that can only be observed in the time domain and can be seen in both the co-polarized and cross-polarized backscattered light in the presence of forward-peaked scattering with $g \geq 0.85$.

2. The electric field Monte Carlo method

Polarized light propagation in turbid media, including human tissues [9], may be described by the time-dependent vector radiative transfer equation (RTE) [10]:

$$(c_o^{-1}\partial_t + \hat{s}\cdot\nabla_r + \sigma_t)\mathbf{I}(\vec{r},\hat{s},t) \quad = \int_\Omega \mathbf{P}(\hat{s}\cdot\hat{s}')\cdot\mathbf{I}(\vec{r},\hat{s}',t)ds' \tag{1}$$

Here $\mathbf{I}$ is the Stokes vector, defined by $\mathbf{I} = (I\ ,Q\ ,U\ ,V)^T$, where T denotes transpose. The components of the Stokes vector are defined in terms of the two orthogonal complex electric field components, $E_{1,2}$, perpendicular to the direction of the incident light: $I = \langle E_1E_1^* + E_2E_2^*\rangle$, $Q = \langle E_1E_1^* - E_2E_2^*\rangle$, $U = \langle E_1E_2^* + E_2E_1^*\rangle$ and $V = i\langle E_1E_2^* - E_2E_1^*\rangle$. $\langle A\rangle$ denotes time averaging of the quantity A, c_o is the speed of light in the medium, σ_t is the total extinction cross section and Ω denotes the unit sphere. $\mathbf{P}$ denotes the 4×4 phase matrix.

Due to the current absence of analytical solutions to the RTE within a bounded medium, numerical studies of polarized light propagation involving Monte Carlo simulation and numerical solutions to the RTE are often the most available tools to explore polarized light propagation in turbid media from a theoretical perspective. These methods [8],[12] - [20] have been extensively used to characterize different types of scattering media such as particle suspensions, and biological materials.

The Electric Field Monte Carlo method (EMC) traces the multiply scattered electric field of incident light in time to simulate the time-resolved propagation of polarized light in turbid media. At each step in time, the EMC program simulates light scattering, absorption, or unhindered propagation giving the scattered electric field, $\mathbf{E}'(t)$. The parallel and perpendicular components of the complex electric field are updated with respect to the instantaneous scattering plane by the amplitude scattering matrix and simultaneous rotations of the local coordinate system spanned by the components of the electric field and the propagation direction. As described in reference [8], if $\mathbf{m}$ and $\mathbf{n}$ are unit vectors in the directions of the parallel and perpendicular components of the electric field with respect to the previous scattering plane and $\mathbf{s}$ is the electric field propagation direction prior to the current scattering event then the propagation direction $\mathbf{s}'$ of the electric field after the current scattering event is given by:

$$\mathbf{s}' = \mathbf{m}\sin(\theta)\cos(\phi) + \mathbf{n}\sin(\theta)\sin(\phi) + \mathbf{s}\cos(\theta) \tag{2}$$

where θ is the scattering angle and ϕ is the azimuthal angle of the current scattering. The current scattering plane is spanned by $\mathbf{s}$ and $\mathbf{s}'$. The unit vectors in the direction of the parallel and perpendicular electric field components with respect to $\mathbf{s}$ and $\mathbf{s}'$ are given prior to scattering

#8479 - $15.00 USD Received 18 August 2005; revised 19 September 2005; accepted 19 September 2005

by:

$$\begin{array}{ll} \mathbf{e}_1 & = \mathbf{m}\cos(\phi) + \mathbf{n}\sin(\phi) \\ \mathbf{e}_2 & = -\mathbf{m}\sin(\phi) + \mathbf{n}\cos(\phi) \end{array} \tag{3}$$

and after scattering are given by:

$$\begin{array}{ll} \mathbf{e}_1' & = \mathbf{m}\cos(\theta)\cos(\phi) + \mathbf{n}\cos(\theta)\sin(\phi) - \mathbf{s}\sin(\theta) = \mathbf{m}' \\ \mathbf{e}_2' & = \mathbf{e}_2 = \mathbf{n}' \end{array} \tag{4}$$

The local coordinate system $(\mathbf{m},\mathbf{n},\mathbf{s})$ is rotated to $(\mathbf{m}',\mathbf{n}',\mathbf{s}')$ with the components of the incident electric field, $\mathbf{E} = E_1\mathbf{m} + E_2\mathbf{n}$, being updated correspondingly by:

$$\mathbf{E}' = E_1'\mathbf{m}' + E_2'\mathbf{n}' = (S_2\mathbf{E}\cdot\mathbf{e}_1)\mathbf{m}' + (S_1\mathbf{E}\cdot\mathbf{e}_2)\mathbf{n}' \tag{5}$$

where $S_2(\theta)$ and $S_1(\theta)$ are the diagonal elements, respectively, of the amplitude scattering matrix. The amplitude scattering matrix is diagonal as a result of the symmetry of the spherical scatterers.

To summarize, the local coordinate system $(\mathbf{m},\mathbf{n},\mathbf{s})$ is updated to $(\mathbf{m}',\mathbf{n}',\mathbf{s}')$ by:

$$\begin{pmatrix} \mathbf{m}' \\ \mathbf{n}' \\ \mathbf{s}' \end{pmatrix} = \begin{pmatrix} \cos(\theta)\cos(\phi) & \cos(\theta)\sin(\phi) & -\sin(\theta) \\ -\sin(\phi) & \cos(\phi) & 0 \\ \sin(\theta)\cos(\phi) & \sin(\theta)\sin(\phi) & \cos(\theta) \end{pmatrix} \cdot \begin{pmatrix} \mathbf{m} \\ \mathbf{n} \\ \mathbf{s} \end{pmatrix} \tag{6}$$

and the electric field is updated by:

$$\begin{pmatrix} E_1' \\ E_2' \end{pmatrix} = \frac{1}{\sqrt{F(\theta,\phi)}} \begin{pmatrix} S_2\cos(\phi) & S_2\sin(\phi) \\ -S_1\sin(\phi) & S_1\cos(\phi) \end{pmatrix} \cdot \begin{pmatrix} E_1 \\ E_2 \end{pmatrix} \tag{7}$$

where the scattered wave intensity, $F(\theta,\phi)$, into direction $\mathbf{s}'$ (characterized by θ,ϕ) has been introduced as a normalizing factor [8]. This normalization factor insures that the scattered light intensity is conserved at each scattering event. Absorption of light is accounted for by adjusting the weight of the scattered photons as in standard Monte Carlo simulations [21].

The coordinate system and electric field are updated simultaneously at each scattering event defined by the sampling of θ,ϕ from the normalized phase function $p(\theta,\phi) = F(\theta,\phi)/\pi Q_{sca}(ka)^2$ where Q_{sca} is the scattering efficiency, k is the wave vector of incident light on a spherical particle and a is the radius of the particle. To sample θ and ϕ the phase function of the particles is determined numerically at the beginning of the calculation.

After n consecutive scattering events the state of a photon is given by the local coordinate system $(\mathbf{m}^{(n)},\mathbf{n}^{(n)},\mathbf{s}^{(n)})$, the complex electric field components $E_{1,2}^{(n)}$, the optical path length l (distance travelled by photon in the medium) and weight, w. Initially unity at incidence, the weight is multiplied by the albedo of the scatterer at each scattering event. Once the photon hits the detector the electric field at the detector, $\mathbf{E}_d$, and Stokes vector, $\mathbf{I}$, is increased according to the detected light increment: $w^{1/2}\mathbf{E}_d = w^{1/2}(E_1^{(n)}\mathbf{m}^{(n)} + E_2^{(n)}\mathbf{n}^{(n)})exp(2\pi il/\lambda)$ [8].

3. Results

A collimated beam, $N\delta(t)\delta(\vec{r})$, where $N = 2\times10^{11}$, of circularly polarized photons with wavelength 632 *nm* is normally incident on a slab of scatterers of length $25[l_s]$. Index-matched boundary conditions are used at the interface of the slab. Mie calculations were used to determine the phase function $p(\hat{s}\cdot\hat{s}')$ and g prior to running the EMC program. The table below lists the size parameter, $2\pi r/\lambda$, and the relative index of refraction of the particle investigated in this study with the specified g factor where r is the radius of each particle and λ is the wavelength of light in the background media. To optimize computation time the calculation was broken up

#8479 - $15.00 USD Received 18 August 2005; revised 19 September 2005; accepted 19 September 2005

Table 1. The size parameters and the relative indices of refraction for scattering spheres of the specified anisotropy factors investigated.

Anisotropy Factor	Size Parameter	Index of Refraction
0.80	3.15	1.1
0.85	3.61	1.1
0.90	4.88	1.1
0.95	7.8	1.1
0.96	10	1.1
0.97	12.1	1.1

into parts involving a reduced number of photons and run simultaneously on the CUNY-GC research cluster. A $50[l_s] \times 50[l_s]$ detecting area with a resolution of $0.1[l_s]$ was used to monitor the light backscattered around the incident direction over a time range of $50[\frac{l_s}{c}]$, with a time resolution of $0.1[\frac{l_s}{c}]$. Two types of collection schemes were explored. The first monitored backscattered light with arbitrary propagation direction and the second collected only light exactly backscattered (propagation direction anti-parallel to the incident beam). Computation time was further reduced by employing the circular symmetry of the spatial profiles of the backscattered light to plot the backscattered intensity as a function of radial distance from the point of incidence. This circular symmetry is attributed to the normal incidence of the beam. All presented results correspond to the collection of backscattered light with arbitrary propagation direction. Each plot of backscattered light intensities, whether spatial or radial, has been normalized by the total number of photons, $N = 2 \times 10^{11}$, used in the simulation.

3.1. Time-resolved backscattering

For time-resolved detection of light backscattered with the same polarization as the incident beam (co-polarized backscatter), a ring centered on the point of incidence of the beam is found to form. Initially the radius of the ring expands linearly with time. The intensity of light at the ring-peak grows weaker as the ring expands. Figure 1 shows the intensity of the co-polarized backscattered beam for $g = 0.96$ at different times. Ring formation corresponds to the red peak which noticeably expands and becomes weaker (as seen in the change in colorbar scales) as time progresses. The backscattered intensity at the ring-peak is more pronounced than backscattering at the point of incidence (the center of the plots). Ring formation was observed in co-polarized backscattered light for all values of g ranging from 0.8 to 0.97.

Figure 2 shows radial profiles of the backscattered intensity with same helicity as the incident beam for g = 0.8, 0.85, 0.9 and 0.95 at a single time $t = 2[\frac{l_s}{c}]$. An important feature illustrated in Fig. 2 is the weakening of the ring-peak as g increases. This is due to increased forward-peaked scattering within the medium and a resulting decrease in the likelihood of return of the photons with polarization of the incident beam.

For each value of g, the ring behavior in the backscattered co-polarized light evolved in a similar way: initially the ring expanded linearly in time away from the point of incidence, growing weaker at each time step, until it reached a maximal radius at which point the ring-peak flattens and backscattering at the point of incidence begins to take over, see Fig. 3. After sufficient time has passed the backscattered light converges to a Gaussian-like distribution with peak at the point of incidence. The maximum radius of the ring and time over which the ring is present (ring-lifetime), increases for increasing values of g, prior to this flattening effect. This

#8479 - $15.00 USD Received 18 August 2005; revised 19 September 2005; accepted 19 September 2005

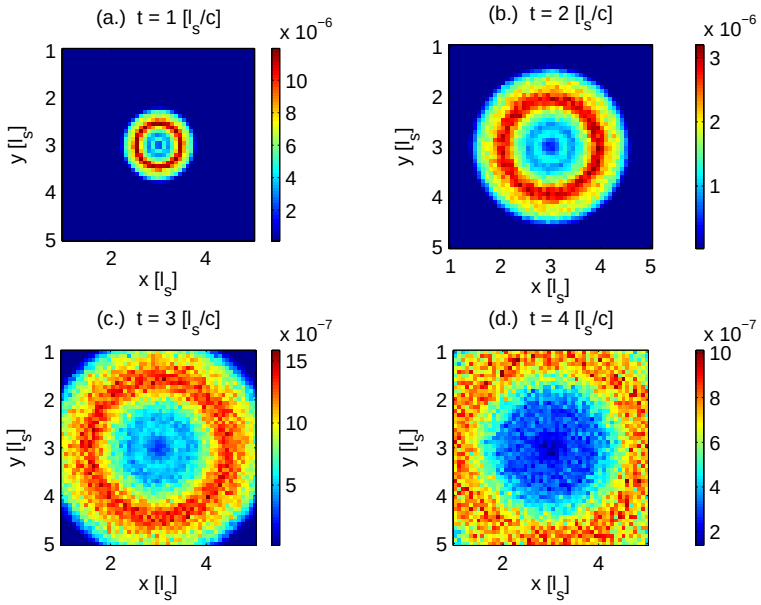

Fig. 1. Backscattered time-resolved intensity of co-polarized light for $g = 0.96$ at times: (a.) t = $1[\frac{l_s}{c}]$, (b.) t = $2[\frac{l_s}{c}]$, (c.) t = $3[\frac{l_s}{c}]$ and (d.) t = $4[\frac{l_s}{c}]$.

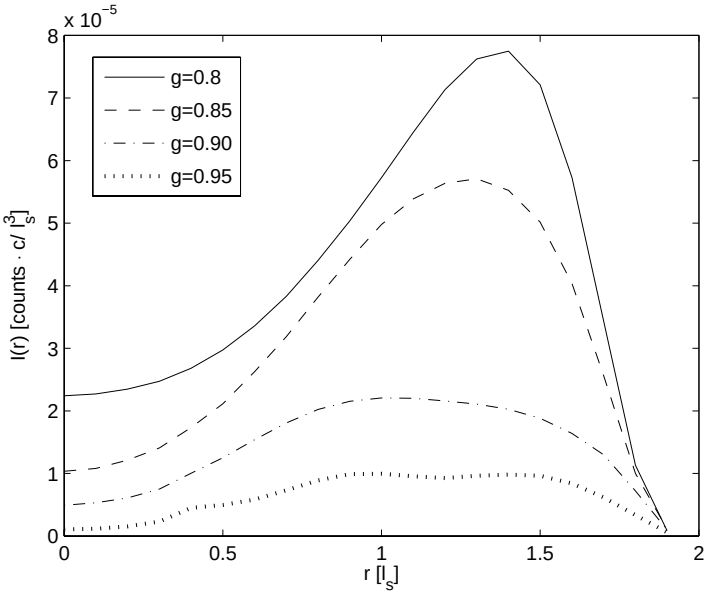

Fig. 2. Comparison of backscattered intensity of light co-polarized with the incident beam for different anisotropy factors at t = $2[\frac{l_s}{c}]$.

#8479 - $15.00 USD Received 18 August 2005; revised 19 September 2005; accepted 19 September 2005

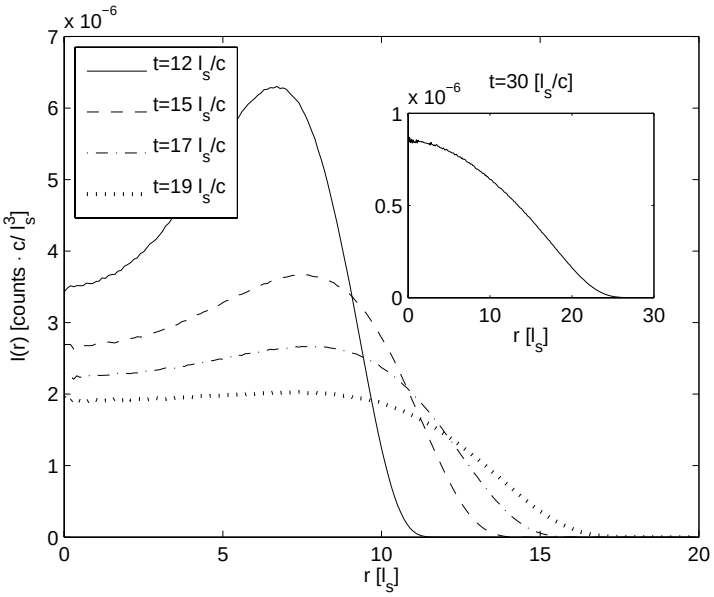

Fig. 3. Time evolution of co-polarized backscattered light for $g = 0.80$. Note at t = $19[\frac{l_s}{c}]$ plateauing of the ring-peak occurs. *Inset:* the radial profile at t = $30[\frac{l_s}{c}]$, convergence to a Gaussian-like distribution.

is a consequence of increased forward scattering as g increases.

The ring behavior occurs due to successive near-forward scattering events which preserve the polarization state of the photon as a result of polarization memory effects [5],[6] described earlier. The successive near-forward scattering events give rise to arc-like trajectories of photons as they travel into the medium. Rings with smaller radii are composed of shallow penetrating photons while rings with larger radii are composed of photons that travel deeper, giving depth information about the scattering medium.

As g increases, the number of near-forward scattering events needed to bring a photon back to the surface increases, giving rise to weaker ring-peaks and prolonged ring life-times. The time-dependence of the rings is a result of photons penetrating deeper into the medium as a result of forward scattering: photons that travel further into the media take longer to backscatter along the semi-circular trajectories giving rise to ring formation at later times. Fig. 4 shows a schematic depiction of this process. Figure 5 shows the linear dependence on time that the ring radius displays up to the point of plateauing of the ring peak. Beyond this plateauing the radial position of the peak of light intensity moves to $r_{max} = 0$ as backscattering at the point of incidence takes over. This feature can be seen in the "fall" back to zero of each curve in Fig. 5. As well, it illustrates the relationship between anisotropy and the duration of the ring behavior of the backscattered light: the ring is prevalent for longer times as g increases.

Light backscattered with the opposite helicity of the incident circularly polarized beam is found to display a different ring-like behavior for sufficiently strong forward-peaked scattering, $g \geq 0.85$. Light is primarily backscattered at the point of incidence, as a result of large angle scattering, with a secondary ring-peak forming some distance away from the point of incidence. As in the case of the helicity preserved backscattered light, the ring radius increases in time and the peak associated with the ring decreases simultaneously.

Figure 6 displays the spatially resolved backscattering of light of opposite helicity with re-

#8479 - $15.00 USD Received 18 August 2005; revised 19 September 2005; accepted 19 September 2005

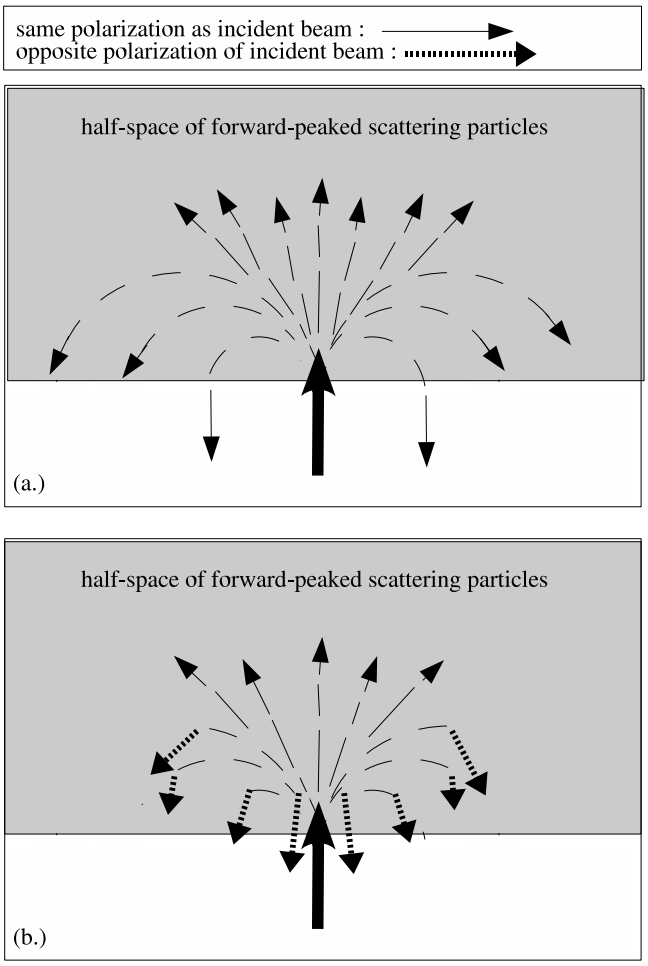

Fig. 4. Schematic diagram illustrating light pathways contributing to ring formation with backscattered light (a.) co-polarized , and (b.) cross-polarized, with the incident beam.

spect to the incident beam (cross-polarized backscatter) for $g = 0.96$. The dark red center of the plots corresponds to backscattering at the point of incidence. The secondary light blue peak is the ring-peak. Light backscattered at the point of incidence results from the finite tail of the phase function, $p(\hat{s} \cdot \hat{s}')$, peaked about the scattering angle $\hat{s} \cdot \hat{s}' = \pi$. Because most of the light is transmitted as a result of forward-peaked scattering, large angle scattering is dominant when looking at the backscattered light. Large angle scattering is also responsible for the helicity flip of the backscattered light [6].

As in the case of polarization preserved backscattering, the ring observed for light backscattered with opposite polarization of the incident beam moves away from the point of incidence as time progresses, growing weaker as it does so, until a plateauing occurs with eventual convergence to a Gaussian-like distribution. Figure 7 displays the plateauing for the case in which $g = 0.85$. The inset displays the Gaussian-like convergence, with peak at the point of incidence, for long times. Again, the ring behavior is attributed to successive near-forward scattering events with the presence of a small number (mostly, single) of large-angle scattering events which are responsible for the polarization flip of the backscattered light, see Fig. 4. Light that

#8479 - $15.00 USD Received 18 August 2005; revised 19 September 2005; accepted 19 September 2005

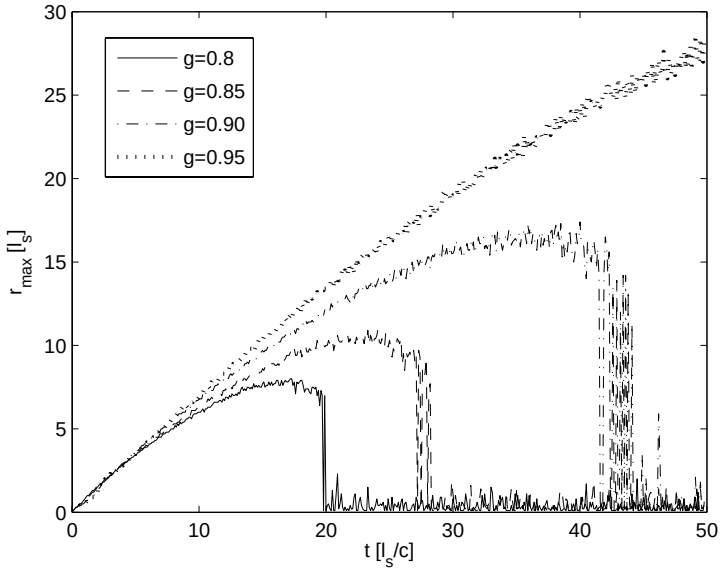

Fig. 5. Time dependence of the radius of the ring-peak of co-polarized backscattered light for various values of *g*.

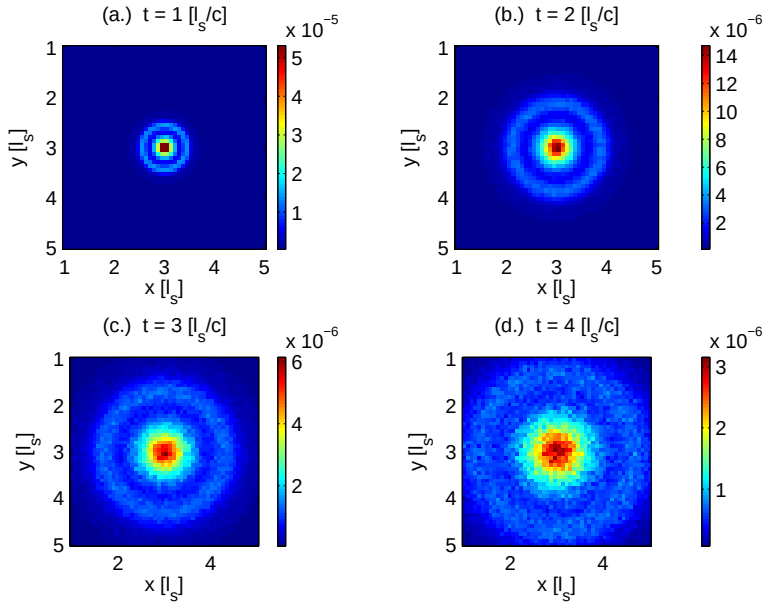

Fig. 6. Time-resolved intensity of cross-polarized backscattered light for $g = 0.96$ at times (a.) t = $1[\frac{l_s}{c}]$, (b.) t = $2[\frac{l_s}{c}]$, (c.) t = $3[\frac{l_s}{c}]$ and (d.) t = $4[\frac{l_s}{c}]$.

#8479 - $15.00 USD Received 18 August 2005; revised 19 September 2005; accepted 19 September 2005

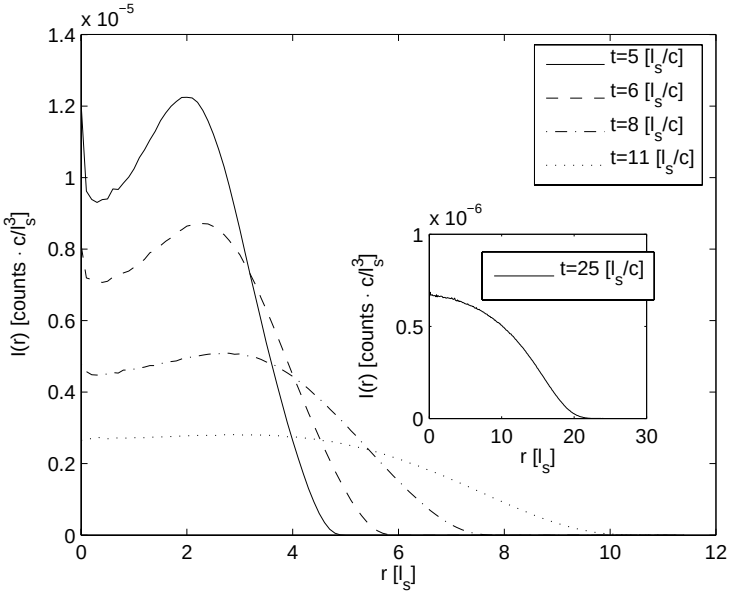

Fig. 7. Time evolution of cross-polarized backscattered light for $g = 0.85$. Note at t = $11[\frac{l_s}{c}]$ plateauing of the ring-peak occurs. Inset: the radial profile at t = $25[\frac{l_s}{c}]$, convergence to a Gaussian-like distribution.

travels deeper into the medium is responsible for ring formation at later times while light that travels to smaller depths is responsible for ring formation at early times. As g increases the ring-peak diminishes due to increased forward scattering resulting in greater transmittance of light, see Fig. 8.

Lastly, a comparison of rings formed by co-polarized and cross-polarized backscattered light at equal times and equal anisotropies reveals that the radial position of ring-peaks composed of light with preserved helicity are greater than the radial position of ring-peaks composed of light with flipped helicity, see Fig. 9. This is attributed to large angle scattering in which photons deviate from the successive near-forward scattering paths comprising the arc-like trajectories going back towards the incident surface. As a result, the photons that undergo large angle scattering towards the incident surface have their polarizations flipped and traverse a shorter path inside the scattering medium, resulting in a smaller ring radius, Fig. 4.

3.2. Continuous-wave backscattering

In the continuous-wave case, no ring formation is observed in the backscattered light of either preserved or flipped helicity with respect to the incident beam. Figure 10 shows the spatially resolved continuous-wave backscattered intensity of both helicities with $g = 0.96$. Backscattering is greatest at the point of incidence of the beam.

The radial profiles for $g = 0.80, 0.85, 0.9$ and 0.95, Fig. 11, as well show no ring formation. Backscattering is dominated at the point of incidence with no ring features.

The absence of ring formation in the continuous wave backscattered light of either helicity is attributed to the dominance of backscattering at the point of incidence at early times. Figures 12 and 13 compare the continuous wave profiles (solid green lines) of preserved and flipped polarizations, respectively, to snap shots of the time-resolved profiles for various times. The continuous wave (time-averaged) profiles have been superimposed on the time-resolved profiles

#8479 - $15.00 USD Received 18 August 2005; revised 19 September 2005; accepted 19 September 2005

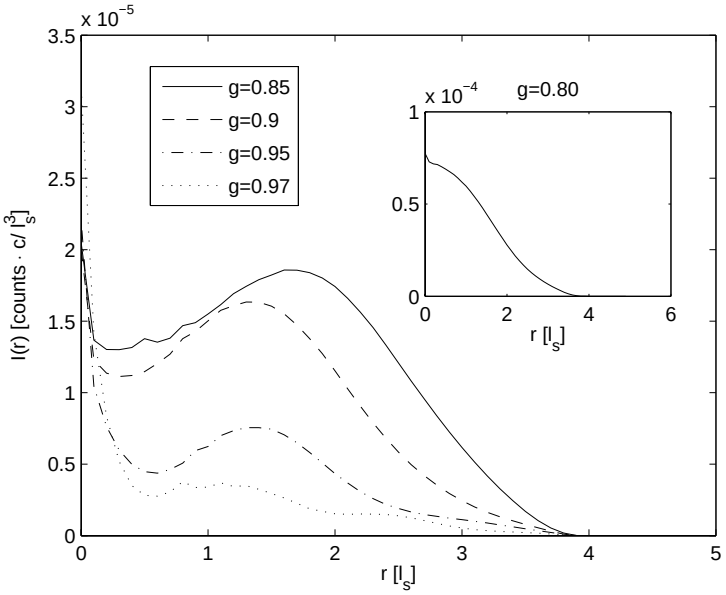

Fig. 8. Comparison of cross-polarized backscattered light for various anisotropies, t = $4[\frac{l_s}{c}]$
.

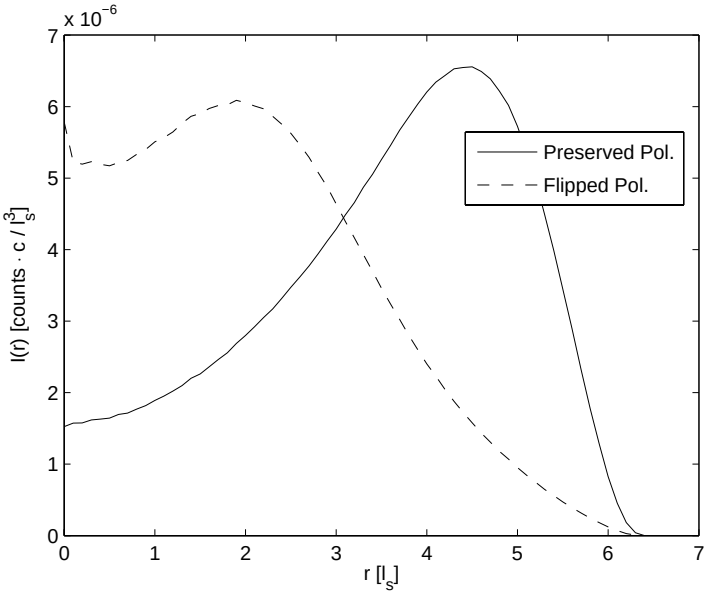

Fig. 9. Comparison of backscattered light with opposite and preserved polarization at t = $6.5[\frac{l_s}{c}]$ and with $g = 0.90$.

#8479 - $15.00 USD Received 18 August 2005; revised 19 September 2005; accepted 19 September 2005

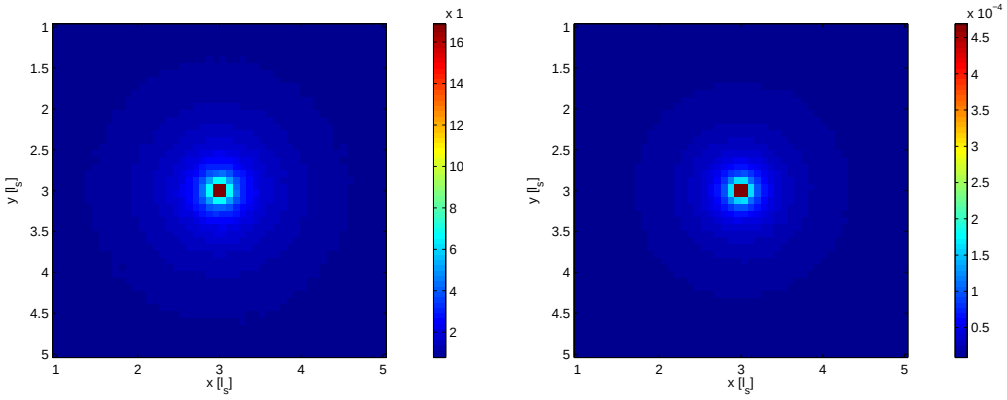

(a) (b)

Fig. 10. Backscattered continuous-wave intensity for (a) co-polarized and (b) cross-polarized light with the incident beam.

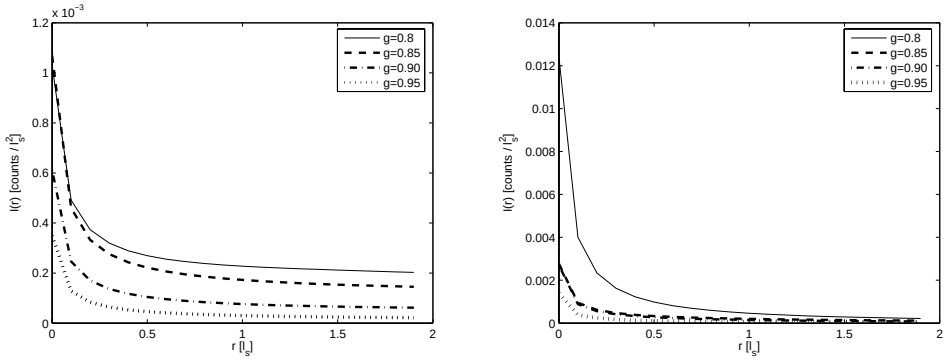

(a) (b)

Fig. 11. Comparison of backscattered continuous-wave intensity for various anisotropies with the same (a) and opposite (b) helicity as the incident beam.

for comparison.

4. Discussion

Ring formation of backscattered light was first described by Kim and Moscoso [7] who predicted a time-independent ring formation using the scalar time-independent Fokker-Planck approximation to radiative transfer in forward scattering media. It was also postulated by these authors that the light composing the ring was of the same helicity of an incident circularly polarized beam. Ring formation was described by Kim and Moscoso as a result of successive near forward scattering events, due to the forward-peaked scattering nature of the particles, which gave rise to a steady state semi-circular trajectory of photons inside the medium. The EMC results presented here suggest partial agreement with Kim and Moscoso however, EMC differs in that it predicts a strictly time-*dependent* ring formation. As well, the EMC results predict ring formation for light backscattered with the same *and* opposite helicity as that of the incident beam.

#8479 - $15.00 USD Received 18 August 2005; revised 19 September 2005; accepted 19 September 2005

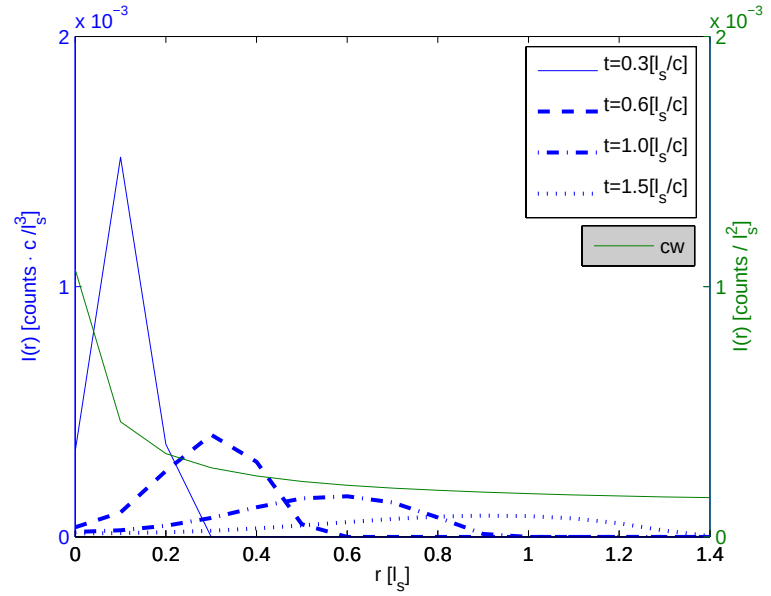

Fig. 12. Comparison of continuous-wave and time-resolved co-polarized backscattered light for $g = 0.85$.

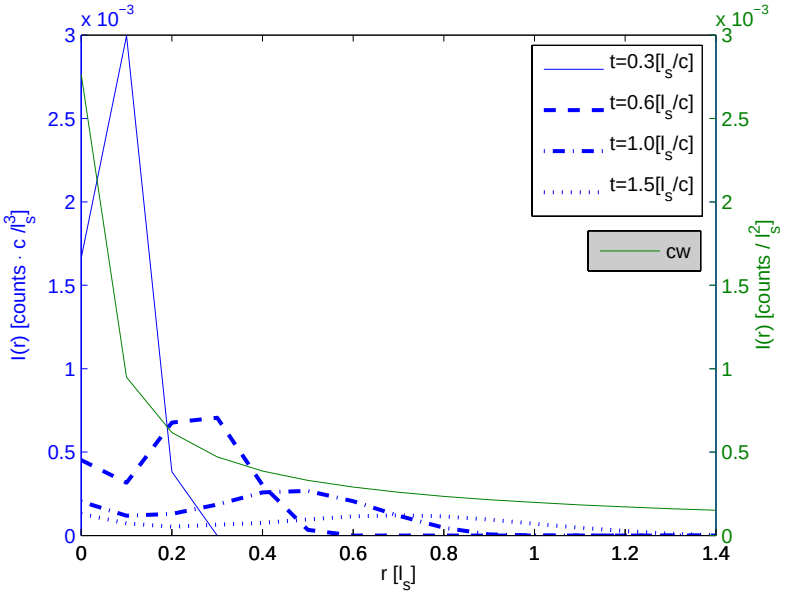

Fig. 13. Comparison of continuous-wave and time-resolved cross-polarized backscattered light for $g = 0.85$.

#8479 - $15.00 USD Received 18 August 2005; revised 19 September 2005; accepted 19 September 2005

The results of the EMC simulation provide a basis for the following explanation of backscattered photon transport in forward-peaked scattering media involving time dependence. In the case of helicity preserved ring formation, the ring peak moves outward away from the point of incidence in time and grows weak simultaneously. This behavior can be understood in terms of successive near forward scattering events in which different amounts of light penetrate deeper into the medium than others, see the schematic in Fig. 4. Light that travels to shallow depths is responsible for ring formation at early times. Due to the forward-peaked nature of scattering, light that travels deeper into the medium is predominantly transmitted with only a small constituent being successively scattered to form arc-like trajectories. This light is responsible for ring formation at later times. This gives rise to an ever widening ring radius and an ever decreasing ring peak as time progresses. It also explains why ring peaks are smaller as g increases. Light is scattered over a smaller distribution of angles about the forward direction increasing the likelihood of transmittance through the slab. As well, the arc-like trajectories become longer as anisotropy increases due to the smaller deviations from the forward direction of the scattering angle resulting in longer ring lifetimes. The ring behaviors described here may be experimentally observed using time-resolved femtosecond pulses using a streak camera or Kerr gate.

In the case of helicity flipped backscattering, light is backscattered with high likelihood at the point of incidence and a secondary ring location. Backscattering at the point of incidence is attributed to the structure of the phase function of the forward-peaked scatterers. There is a finite peak in the phase function about the scattering angle π giving rise to a finite probability of backscatter with helicity flip. Because photons are primarily transmitted due to the forward-peaked nature of scattering, light scattered through a large angle dominates when analyzing backscatter. Ring formation in this case is a result of forward-peaked scattering events combined with large angle scattering events. Forward-peaked scattering brings about the ring behavior while large angle scattering at some point along the photon's trajectory is responsible for the helicity flip of the photon and the decreased ring radius, see Fig. 9. For values of $g < 0.85$, off-forward scattering remains dominant to the point of quenching opposite helicity ring formation when collecting backscattered light with arbitrary propagation direction. As a result, backscatter is dominant at the point of incidence with a Gaussian-like distribution as distance from the central point of incidence increases.

The analysis of continuous-wave backscattered light revealed an absence of ring formation. This can be reconciled with the time-dependent nature of ring formation presented above by recognizing that the time integration destroys the ring structure. It is noted that the dependence of ring formation on the collection angle of backscattered light is weak in the presence of high anisotropy, $g \geq 0.85$. When scattering becomes more isotropic it is expected that ring formation will first be observed when collecting light exactly backscattered anti-parallel to the incident beam. The ring behavior can be observed when collecting light of both preserved and flipped polarizations simultaneously, Fig. 14.

Finally it is noted that the discrepancy between the EMC results and the results of Kim and Moscoso [7] can be traced to the differing phase functions employed in each study. Kim and Moscoso used an exponential phase function peaked at the exact forward scattering direction. This phase function allows only nearly forward scattering events and no large angle scattering. The phase function for naturally occurring scatterers, including biological tissues, may not decay exponentially as the scattering angle deviates from the forward direction and furthermore has a tail at larger scattering angles. The EMC method employs the exact Mie phase function of the spherical scatterers which even in the limit of strong forward scattering possesses a small but finite tail at large angles. The small yet finite probability for light scattering with large angles indeed gives rise to a peak in the backscattered light at the point of incidence at early

#8479 - $15.00 USD Received 18 August 2005; revised 19 September 2005; accepted 19 September 2005

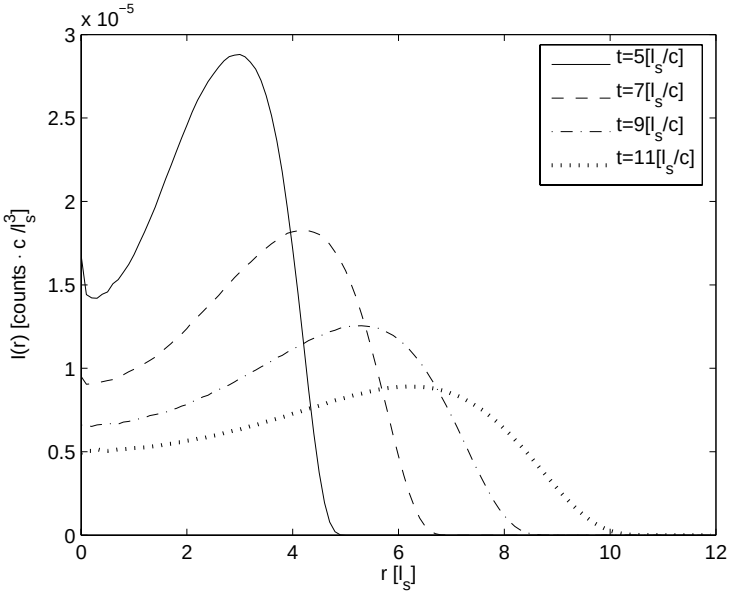

Fig. 14. Time evolution of simultaneous collection of co-polarized and cross-polarized backscattered light for $g = 0.85$.

times, see Fig. 12 and 13. It is the predominance of backscattering at early times near the point of incidence which prevents ring formation in the steady-state case.

5. Conclusion

The EMC method was used to investigate the backscattering of circularly polarized light at normal incidence to a half-space of forward scattering particles ranging in anisotropies of $g = 0.8$ to $g = 0.95$. The spatial dependence of the backscattered intensity is examined for both the time-resolved and continuous-wave cases. Time-resolved analysis reveals ring formation for *both* co-polarized *and* cross-polarized backscattered light for $g \geq 0.85$. For values of $g < 0.85$, off-forward scattering remains dominant to the point of quenching ring formation when collecting backscattered light with arbitrary propagation direction and opposite polarization with respect to the incident beam. Ring behavior is similar in both types of backscattered light: the ring radius grows in time with the ring-peak decreasing simultaneously. The ring pattern is more pronounced when light is backscattered with the same polarization as the input. For the continuous-wave case, no such ring is observed. The ring formation presented in this study provides an important clue for understanding how light is backscattered from forward scattering media. Specifically, the EMC results suggest that photons undergo successive near-forward scattering events. Furthermore, these findings suggest that backscattered light is comprised of photons undergoing arc-like trajectories within the medium. In addition, the photons penetrate to different depths such that rings that form near the point of incidence of the pencil-like beam (at early times) are comprised of photons that have penetrated to smaller depths while rings that form further away from the point of incidence (at later times) are comprised of deeper penetrating photons. This knowledge may have potential use in polarization imaging techniques to acquire depth information of targets. Ring formation with cross-polarized backscattered light arises from successive forward-peaked scattering events over most of the photons path with

#8479 - $15.00 USD Received 18 August 2005; revised 19 September 2005; accepted 19 September 2005

large angle scattering events taking place at some point along the trajectory to flip the photon's helicity. It is the large angle scattering events which give rise to smaller ring radii than in the case of light backscattered with preserved polarization. It is noted that these results come in contrast to previous theoretical studies of backscattered light using the scalar time-independent Fokker-Planck approximation to radiative transfer [7] which predict a continuous-wave ring formation. The results given by the EMC method suggest that the time dependence and polarization state of the scattered light intensities play a crucial role in understanding ring formation for forward scattering media.

Acknowledgments

The authors thank Dr. Florian Lengyel, Assistant Director for Research Computing at the CUNY-GC computing facilities, for extensive help and support using the CUNY-GC research cluster. The authors acknowledge helpful discussions with Dr. Wei Cai. This research was supported in part by ONR Award No: N00014-03-1-0463 and by NASA COSI.

#8479 - $15.00 USD Received 18 August 2005; revised 19 September 2005; accepted 19 September 2005